Spin-orbit interaction driven collective electron-hole excitations in a non-centrosymmetric nodal loop Weyl semimetal

Kyo-Hoon Ahn[1], Kwan-Woo Lee[1,2],* and Warren E. Pickett[3†]
[1] *Department of Applied Physics, Graduate School, Korea University, Sejong 339-700, Korea*
[2] *Department of Display and Semiconductor Physics, Korea University, Sejong 339-700, Korea*
[3] *Department of Physics, University of California, Davis, CA 95616, USA*
(Dated: July 13, 2015)

NbP is one member of a new class of nodal loop semimetals characterized by the cooperative effects of spin-orbit coupling (SOC) and a lack of inversion center. Here transport and spectroscopic properties of NbP are evaluated using density functional theory methods. SOC together with the lack of inversion symmetry splits degeneracies, giving rise to "Russian doll nested" Fermi surfaces containing 4×10^{-4} electron (hole) carriers/f.u. Due to the modest SOC strength in Nb, the Fermi surfaces map out the Weyl nodal loops. Calculated structure around T$^*\approx$100 K in transport properties reproduces well the observed transport behavior only when SOC is included, attesting to the precision of the (delicate) calculations and the stoichiometry of the samples. Low energy collective electron-hole excitations (plasmons) in the 20-60 meV range result from the nodal loop splitting.

PACS numbers: 71.20.Be,71.18.+y,78.20.Ci,72.15.Eb

Weyl semimetals have Weyl points, comprised of a linear crossing of valence and conduction bands[1] near the Fermi energy E$_F$. Weyl semimetals can be realized from a lack of time-reversal symmetry (magnetic ordering, or applied field B),[1–3] or from no inversion symmetry in 3-dimensional compounds,[4, 5] and show peculiar features, such as Fermi arcs from surface states connecting two Weyl points with different chirality.[1, 4, 5] Experimental evidence has been obtained using x-ray angle-resolved photoemission spectroscopy.[6] Extremely large magnetoresistivity (XMR) also occurs in some Weyl semimetals, with a recent analysis by Burkov[3] concluding that XMR should be expected in high mobility semimetals where Weyl or Dirac points lie near the Fermi surface (FS). XMR was observed also in the semimetal WTe_2, showing unsaturated MR up to 60 T,[7] attributed to precise electron and hole carrier compensation, as in Bi and other stoichiometric semimetals.

Recently a "nodal loop" Weyl semimetal phase with potentially distinctive properties has been proposed on theoretical grounds[4, 5] in the nonmagnetic non-centrosymmetric compounds TaAs, TaP, NbAs, and NbP. Since these suggestions, XMR has been observed in both TaAs[8, 9] and NbP.[9, 10] NbP, upon which we focus here, shows XMR of 8,500 at 2 K for $B = 9$ T, increasing to 3×10^4 at 4 K at B=30 T, to 10^5 at 60 T, and remains unsaturated.[10] These colossal XMR values reflect the excellent conduction at low temperatures, with resistivity as low as $0.1\mu\Omega$ cm, and a metal to insulator crossover with field at 100 K and below. A high mobility μ=5×10^6 cm^2/V-s and carrier density of 1.5×10^{18} cm^{-3} at low T was inferred from the conventional single band expressions, which however are not quantitative for multiband semimetals. As temperature increases, both the Hall coefficient R_H changes sign from electron-like to hole-like and the mobility rapidly changes in the 50-150 K range, correlating with the metal to insulator crossover. A multiband model and additional data will be necessary to sort out individual carrier densities and mobilities.

From both theoretical and experimental viewpoints, nodal loop semimetals comprise a new class of materials with topological behavior. In this paper we focus on effects of spin-orbit coupling (SOC) on the electronic properties and evaluate the optical and transport coefficients of NbP, using density functional theory based methods that enable a direct theory-experiment comparison. A central feature that emerges is electronic fine structure driven by the combination of SOC and lack of an inversion center, a feature elaborated on by Samokhin.[11] This splitting in a semimetal with small closed Fermi surfaces FSs results in "Russian doll nested" pair of FSs, and new low energy interband transition strength pilfered from the Drude strength by non-centrosymmetry. The FS character is clarified and low energy collective electronic excitations (plasmons) arising from the electronic fine structure are predicted. While plasmons have been studied in ideal Weyl semimetals,[12–15] this and several other properties are distinct in a "nodal loop semimetal" such as NbP.

Structure and Theoretical Methods. NbP has a body-centered tetragonal lattice of the space group $I4_1md$ (#109).[16] This space group has $4mm$ point group, is non-symmorphic, and (importantly) lacks inversion symmetry. The structure can be pictured as columns of face-shared NbP_6 trigonal prisms oriented along the $\hat{a}$-axis, edge-shared along the $\hat{b}$-axis in one layer. The trigonal columns are 90° rotated in the next layer along the $\hat{c}$-axis, giving overall tetragonal symmetry. In the structure with the experiment lattice parameters[16] of $a = 3.3324$ Å, $c = 11.3705$ Å, both Nb and P ions lie at $4a$ posi-

*Electronic address: mckwan@korea.ac.kr
†Electronic address: pickett@physics.ucdavis.edu

tions $(0, 0, z)$: $z_{Nb} = 0$, z_P=0.4176; the site symmetry is $2mm$. Our optimized positions using the generalized gradient approximation (GGA) with the Perdew-Burke-Ernzerhof (PBE) exchange-correlation functional[17] in FPLO[18] coincided with the experimental values. This structure leads to nearly identical Nb-P bond lengths of 2.53±0.01 Å and P-Nb-P bond angles around 82°.

Calculations with the experiment structure were performed using the all-electron full-potential code WIEN2K,[19] with selected results confirmed with FPLO. All results are based on the PBE-GGA exchange-correlation functional. One objective is to determine the combined effects of SOC and the lack of inversion center, since delicate features around E_F are sensitive to SOC and become important.

Calculation of optical properties including SOC is available in WIEN2K.[20] The dielectric function $\epsilon_{ij}(\omega)$, with only diagonal $\epsilon_{aa} = \epsilon_{bb}$ and ϵ_{cc} components due to tetragonal symmetry, is decomposed into the intra- and inter-band contributions. The imaginary parts of each contribution are given by[20, 21]

$$Im\epsilon_{jj}^{intra}(\omega) \propto \frac{\Gamma\Omega_{p,jj}^2}{\omega(\omega^2+\Gamma^2)}, \quad (1)$$

$$Im\epsilon_{jj}^{inter}(\omega) \propto \sum_{c,v}\int d\vec{k}\frac{|\langle c_{\vec{k}}|p_j|v_{\vec{k}}\rangle|^2}{\omega^2}\delta(\varepsilon_{c_{\vec{k}}}-\varepsilon_{v_{\vec{k}}}-\omega),$$

where $\vec{p}$ is the momentum operator, and $\varepsilon_{c_{\vec{k}}}$ and $\varepsilon_{v_{\vec{k}}}$ are energies of the occupied $v_{\vec{k}}$ and unoccupied $c_{\vec{k}}$ orbitals, respectively. In the intraband term, which contains the Drude divergence for $\omega \to 0$, $\Omega_{p,jj}$ is the Drude plasma frequency and Γ (chosen to be 10 meV here) is an inverse scattering lifetime τ. The corresponding real parts are obtained by the Kramers-Kronig relation.

The transport calculations were carried out using semiclassical Bloch-Boltzmann transport theory, implemented in the BOLTZTRAP code[22] that is interfaced to WIEN2K. No approximations beyond the constant scattering time approximation are made. In all calculations performed here, the Brillouin zone was sampled with a dense k-mesh up to $60\times60\times60$ to treat the semimetallic fine structure carefully. In WIEN2K, the basis size was determined by $R_{mt}K_{max} = 8$, and augmented plane-wave sphere radii of 2.5 Bohr (Nb) and 2.14 Bohr (P) were used.

Electronic fine structure. We first address the electronic structure obtained with fine k-point and energy meshes. Figure 1 shows the GGA and GGA+SOC band structures near E_F. Semimetallic character with a band crossing along at least three symmetry directions appears, with valence-conduction overlaps mostly of the order of 150 meV. This band behavior leads to a pseudogap centered 20 meV below E_F (Fig. 1), with a very small density of states (DOS) $N(E_F)$=0.046 states/eV per f.u. While these results are similar to the previous report,[4, 10] we examine the origins and consequences more completely.

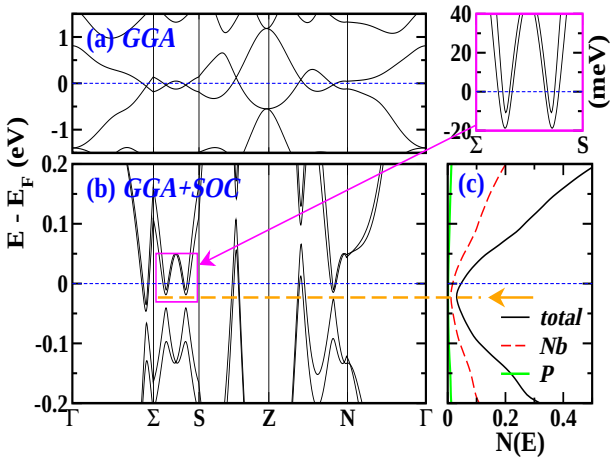

FIG. 1: (color online) (a) GGA bands in the range of -1.5 eV to 1.5 eV and (b) GGA+SOC bands in the range of -0.2 eV to 0.2 eV, with E_F set to zero. The symmetry points can be identified in Fig. 2. The upper right panel enlargement shows the splitting by ∼10 meV of bands by SOC in this non-centrosymmetric structure. (c) Density of states (GGA+SOC) showing the pseudogap centered 20 meV below E_F.

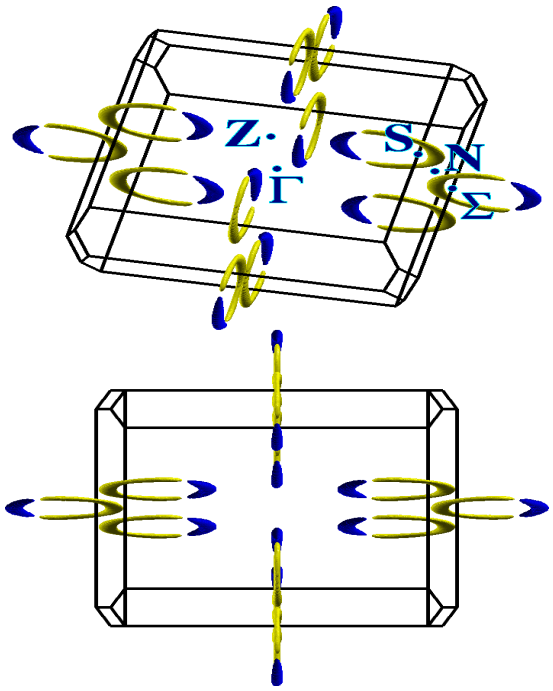

FIG. 2: (color online) NbP Fermi surfaces (FSs) including SOC and shown from two angles, the lower one viewed along the k_x axis to reveal the thinness of the surfaces in the mirror planes. The extended zone representation makes the toroidal origin of the FSs evident. The hole (blue) FSs form bent and 'sharply' tipped boomerang surfaces, the electron (yellow) surfaces are similar but extend over a larger angle of the torus.

Inclusion of SOC leads to unconventional consequences. As usual, SOC converts many band crossings along symmetry lines into anticrossings; here gapping bands by a few tens of meV near E_F. However, the lack of inversion symmetry leads to lifting of band degeneracy over entire symmetry planes,[4] with splittings in the 20-200 meV range. In spite of the modest magnitude of SOC in 4*d* Nb, SOC will play an important role in determining both the thermal and spectroscopic properties of NbP.

Fermi surfaces. The FSs obtained from GGA+SOC are displayed in Fig. 2, see the caption for description. They are similar to those presented earlier, but are displayed in an extended zone manner to illustrate their toroidal origin. Weng *et al.* have described in detail[4] the underlying features of the Weyl nature of NbP and isovalent partner compounds. Without SOC, mirror symmetry protected nodal loops lie precisely in the mirror planes $k_x = 0$ and k_y=0. The nodal loops consist of band degeneracies $\varepsilon_{1,s}(\vec{k}) = \varepsilon_{2,s}(\vec{k})$ (s is spin degeneracy). The locus of $\vec{k}$ points at this intersection forms the ring in the ΓZN mirror plane, not at constant energy but, for these compounds, in a small energy range including E_F. The FS intersects the nodal loop, so it must include an even number of doubly degenerate *Fermi points* where $\varepsilon_{1,s}(\vec{k}) = \varepsilon_{2,s}(\vec{k}) = E_F$. Such nodal loops have also been found in two dimensional $SrVO_3$ nanolayers.[23]

In this non-centrosymmetric structure, SOC splits the bands forming the nodal loops, leaving two symmetry-inequivalent pairs of Weyl points (12 in all) near but not on the FSs, the points being provided explicitly by Weng *et al.*[4] One lies in the $k_z = 0$ plane, the other at a general $\vec{k}$ point lying near the ΓNZ plane. The band splitting is highly anisotropic; each FS (Fig. 2) consists of a flattened torus (annulus) pinched off into one "boomerang" containing holes and one "new moon" containing electrons. Small doping will alter the position of the pinching, hence changing the number of electron and hole carriers.

For a stoichiometric compound the FSs contain an equal number of holes and electrons, and from calculated band fillings we obtain 4.2×10^{-4} electron (hole) carriers per f.u. This value corresponds to high velocity carriers of each sign separated on average by 13 lattice constants in each direction. The rms Fermi velocities are $v_{F,aa}$=3.7, $v_{F,cc}$=1.6, in 10^7 cm/s, a factor of 2.35 in anisotropy. Note that the velocities are typical of *metallic* compounds, not semimetals, due to the dispersive bands crossing E_F, *i.e.* the Weyl character (analogous to graphene). For the Drude plasma energy, the semimetallic value of $N(E_F)$ but normal metal velocities lead to $\Omega_{p,aa}$=1.0 eV, $\Omega_{p,cc}$=0.4 eV.

What cannot be seen in Fig. 2 is the doubling of the FSs resulting from the interplay of SOC with the non-centrosymmetric crystalline symmetry. With the band degeneracy split, Fermi surfaces become "Russian doll nested" pairs, one inside the other. This band-splitting effect has been discussed for Pt-based superconductors[24] and for electronic properties more generally.[11] The band spitting aspect is effective both in k-space (nested Fermi surfaces) and in energy, with consequences discussed below.

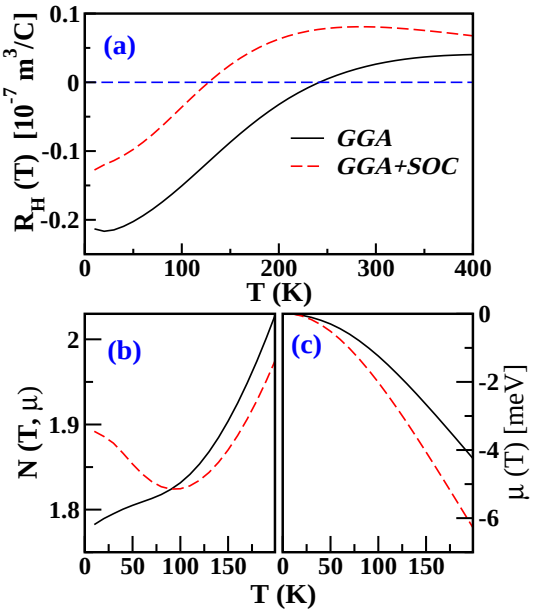

FIG. 3: (color online) (a) Temperature (T) dependent Hall coefficients $R_H(T)$ calculated in both GGA and GGA+SOC, which show similar T-dependence but distinctions in the zero crossing temperature; T=125 K in GGA+SOC, compared to T=230 K in GGA. (b) T-dependent total density of states $N(T,\mu)$ at chemical potential $\mu(T)$. $N(T,\mu)$ shows a minimum around T=100 K in GGA+SOC, while that of GGA increases as increasing T. (c) $\mu(T)$ with respect to E_F at T=0 K.

Transport properties. The transport behavior is very sensitive to Fermiology and the regions of high curvature, but calculated values are in very good agreement with observed behavior.[10] The Hall tensor components $R_H(T)$ including SOC, displayed in Fig. 3(a), show a change in sign at T_c=125 K, precisely where the experimental R_H changes sign.[10] This change of sign is a strong reminder that in a multiband, compensated semimetal, R_H bears no relation to carrier densities.[25] The experiment-theory agreement reflects not only the precision of the calculations but also the excellent stoichiometry of the samples; the stoichiometry could not be established precisely but is supported also by the high mobility. The magnitude of $R_H(T)$ around 250 K is within a factor of two of the experimental value, note that there is large cancellation in the evaluation of R_H, which is the average of curvatures of the FSs. The experimental R_H becomes at the lowest temperature two orders of magnitude larger in magnitude than our calculated value, and it is clear from the "pointed" FSs in Fig. 2 that evaluating R_H (which is an average of the FS curvature) at T=0

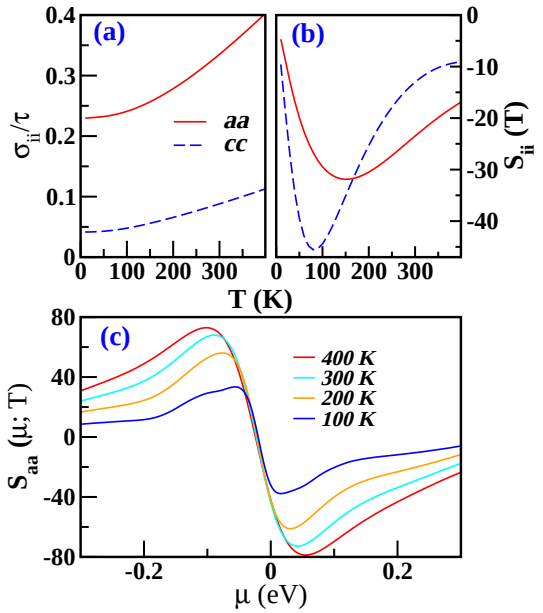

FIG. 4: (color online) Temperature and polarization dependent (a) conductivity tensor, in 10^{20} $(\Omega\text{-m-s})^{-1}$, and (b) Seebeck coefficients S_{ii} [μV/cm], note the minimum in the latter in the 100-150 K range. (c) The Seebeck coefficient $S_{aa}(\mu;T)$ versus band filling μ at various temperatures, within GGA+SOC. The change at very small levels of doping is extremely rapid, reflecting the movement away from charge compensation; S_{cc} behaves in the same manner. The temperature variation is monotonic.

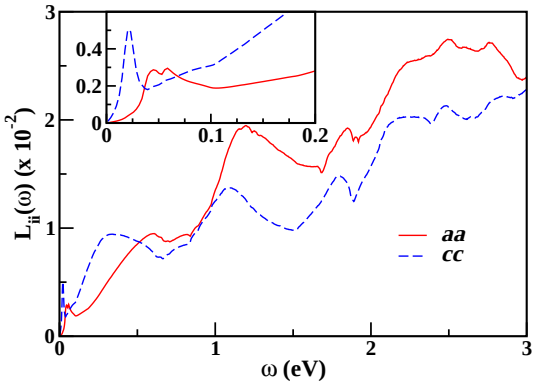

FIG. 5: (color online) The polarization-dependent energy loss function for NbP assuming a scattering rate $\Gamma = \hbar/\tau$ of 10 meV. Inset: the $\hat{c}$-axis plasmon at 20 meV bifurcates into a pair of plasmons at 40 meV and 60 meV for in-plane polarization. Above 0.2 eV the loss function is not greatly anisotropic and is insensitive to Γ.

is a substantial numerical challenge.

The chemical potential $\mu(T)$, displayed in Fig. 3(c), decreases with increasing T. This change is different in sign from another XMR compound WTe_2,[26] reflecting different DOSs of the valence and conduction bands. The DOS at chemical potential $N(\mu)$, shown in Fig. 3(b), is reduced and achieves a minimum around 100 K before turning around. Figure 4(a) displays the conductivity tensor components σ_{ii}/τ which show the anisotropy of $\Omega_{p,jj}$, being $\sim$5 times larger in-plane.

The T-dependent Seebeck coefficients, shown in Fig. 4(b), have net n-type sign. They peak (in magnitude) at 100-150 K before again becoming small. The dependence on chemical potential μ, which can be varied by doping or by gating, is extremely strong near stoichiometry [see Fig. 4(c)]. The near-perfect cancellation of electron and hole contributions (it is perfect $S_{jj} = 0$ for $\mu\approx$-15 meV) at stoichiometry is destroyed, with a maximum of $|S(\mu)|$ being attained around 0.5% hole doping, or half of that for electron doping. The sensitivity makes the thermopower an important gauge of the degree of stoichiometry of samples, which otherwise can be very difficult to determine as this low level.

Optical properties. The band splitting induced by SOC and the lack of inversion symmetry have qualitative consequences for the optical properties. The energy loss function, shown in Fig. 5 with Γ=10 meV, displays low energy plasmons when SOC is included, at 20 meV for $\hat{c}$-axis polarization and double in-plane plasmon peaks at 40 meV and 60 meV. The strength of these peaks, and to some degree their positions, are dependent on the scattering rate Γ. The peaks can be expected also to have temperature dependence, because the varying $\mu(T)$ induces changes and Γ will be T-dependent as well. Above 200 meV, we do not expect significant T-dependence of the spectral behavior.

Discussion and Summary. Our study has illuminated the origins of the unusual Fermi surfaces of NbP. Without consideration of spin-orbit coupling, the electronic structure includes nodal loops[4] lying in the mirror planes that lead to point Fermi surfaces as well as small electron and hole pockets. In this non-centrosymmetric structure, spin-orbit coupling removes the spin degeneracy, resulting in Russian doll nested pairs of Fermi surfaces of a pinched-off annulus topology, with electron surfaces converting to hole surface across the pinch. The resulting electronic fine structure accounts well for the change in sign of the Hall coefficient at 100 K, which is also the temperature range in which the magnetoresistance begins to grow in size. The unusual Fermi surface also accounts for the lack of universal scaling of XMR in NbP and TaP; spin-orbit coupling is much larger in TaP and the Fermi surfaces are sensitive to this. Finally, the fine structure in NbP results in the appearance of polarization dependent low energy plasmons in the 20-60 meV range. This study substantially broadens the understanding of how Weyl semimetal behavior impacts the physical properties of NbP, which should also apply to NbAs, TaP, and TaAs.

Acknowledgments. We acknowledge J.-G. Hong for

useful communications on magnetoresistance and A. S. Botana for useful discussion on calculations in BoltzTraP. This research was supported by National Research Foundation of Korea Grant No. NRF-2013R1A1A2A10008946 (K.H.A and K.W.L), by U.S. National Science Foundation Grant DMR-1207622-0 (K.W.L.) and by U.S. Department of Energy Grant DE-FG02-04ER46111 (W.E.P.).

[1] X. Wan, A. M. Turner, A. Vishwanath, and S. Y. Savrasov, Topological semimetal and Fermi-arc surface states in the electronic structure of pyrochlore iridates. Phys. Rev. B **83**, 205101 (2011).

[2] G. Xu, H. Weng, Z. Wang, X. Dai, and Z. Fang, Chern semimetal and the quantized anomalous Hall effect in $HgCr_2Se_4$. Phys. Rev. Lett. **107**, 186806 (2011).

[3] A. A. Burkov, Chiral anomaly and transport in Weyl metals. J. Phys.: Condens. Matter **27**, 113201 (2015).

[4] H. Weng, C. Fang, Z. Fang, A. Bernevig, and X. Dai, Weyl semimetal phase in noncentrosymmetric transition-metal monophosphides. Phys. Rev. X **5**, 011029 (2015).

[5] S.-M. Huang, S.-Y. Xu, I. Belopolski, C.-C. Lee, G. Chang, B.K. Wang, N. Alidoust, G. Bian, M. Neupane, C. Zhang, S. Jia, A. Bansil, H. Lin, and M. Z. Hasan, A Weyl Fermion semimetal with surface Fermi arcs in the transition metal monopnictide TaAs class. Nature Commun. **6**, 7373 (2015).

[6] B. Q. Lv, N. Xu, H. M. Weng, J. Z. Ma, P. Richard, X. C. Huang, L. X. Zhao, G. F. Chen, C. Matt, F. Bisti, V. Strokov, J. Mesot, Z. Fang, X. Dai, T. Qian, M. Shi, and H. Ding, Observation of Weyl nodes in TaAs. arXiv:1503.09188 (2015).

[7] M. A. Ali, J. Xiong, S. Flynn, J. Tao, Q. D. Gibson, L. M. Schoop, T. Liang, N. Halddolaarachchige, M. Hirschberger, N. P. Ong, and R. J. Cava, Large, non-saturating magnetoresistance in WTe_2. Nature **514**, 205 (2014).

[8] C. Zhang, Z. Yuan, S. Xu, Z. Lin, B. Tong, M. Z. Hasan, J. Wang, C. Zhang, and S. Jia, Tantalum monoarsenide: an exotic compensated Semimetal. arXiv:1502.00251 (2015).

[9] C. Zhang, C. Guo, H. Lu, X. Zhang, Z. Yuan, Z. Lin, Large magnetoresistance over an extendded temperature regime in monophosphides of tantalum and niobium, arXiv:1507,01298.

[10] C. Shekhar, A. K. Nayak, Y. Sun, M. Schmidt, M. Nicklas, I. Leermakers, U. Zeitler, W. Schnelle, J. Grin, C. Felser, and B. Yan, Extremely large magnetoresistance and ultrahigh mobility in the topological Weyl semimetal candidate NbP. Nature Phys. **online** doi:10.1038/nphys3372 (2015).

[11] K. V. Samokhin, Spin-orbit coupling and smeiclassical electron dynamics in noncentrosymmetric metals. Ann. Phys. **324**, 2385 (2009).

[12] M. Lv and S.-C. Zhang, Dielectric function, Friedel oscillation, and plasmons in Weyl semimetals. Intl. J. Mod. Phys. B **27**, 1350177 (2013),

[13] I. Panfilov, A. Burkov, and D. A. Pesin, Density response in Weyl metals. Phys. Rev. B **89**, 245103 (2014).

[14] J. Zhou, H.-R. Chang, and D. Xiao, Plasmon mode as a detection of the chiral anomaly in Weyl semimetals. Phys. Rev. B **91**, 035114 (2015),

[15] J. Hofmann and S. Das Sarma, Plasmon signature in Dirac-Weyl liquids. Phys. Rev. B **91**, 241108 (2015).

[16] J. Xu, M. Greenblatt, T. Emge, P. Höhn, T. Hughbanks, and Y. Tian, Crystal structure, electric transport, and magnetic properties of niobium monophosphide. Inorg. Chem. **35**, 845 (1996).

[17] J. P. Perdew, K. Burke, and M. Ernzerhof, Generalized gradient approximation made simple. Phys. Rev. Lett. **77**, 3865 (1996).

[18] K. Koepernik and H. Eschrig, Full-potential nonorthogonal local-orbital minimum-basis band-structure scheme. Phys. Rev. B **59**, 1743 (1999).

[19] K. Schwarz and P. Blaha, Solid state calculations using WIEN2k. Comput. Mater. Sci. **28**, 259 (2003).

[20] C. Ambrosch-Draxl and J. O. Sofo, Linear optical properties of solids within the full-potential linearized augmented planewave method. Comput. Phys. Commun. **175**, 1 (2006).

[21] Y. Li, K. Foyevtsova, H. O. Jeschke, and R. Valentí, Analysis of the optical conductivity for A_2IrO_3(A=Na, Li) from first principles. Phys. Rev. B **91**, 161101(R) (2015).

[22] G. K.H. Madsen and D. J. Singh, BoltzTraP. A code for calculating band-structure dependent quantities. Comput. Phys. Commun. **175**, 67 (2006).

[23] V. Pardo and W. E. Pickett, Electron Confinement, Orbital Ordering, and Orbital Moments in $d^0 - d^1$ Oxide Heterostructures, Phys. Rev. B **81**, 245117 (2010).

[24] K.-W. Lee and W. E. Pickett, Crystal symmetry, electron-phonon coupling, and superconducting tendencies in Li_2Pd_3B and Li_2Pt_3B. Phys. Rev. B **72**, 174505 (2005).

[25] The Hall coefficient does not however give a reliable carrier density in a multiband, compensated electron-hole semimetal, as mentioned by Shekhar *et al.*[10]

[26] Y. Wu, N. H. Jo, M. Ochi, L. Huang, D. Mou, S. L. Bud'ko, P. C. Canfield, N. Trivedi, R. Arita, and A. Kaminski, Temperature induced Lifshitz transition in WTe_2. arXiv:1506.03346.